

Article

Tuning Growth of ZnO Nano-Arrays by the Dewetting of Gel Layer

Ziqian Li, Ningzhe Yan, Yangguang Tian and Hao Luo * 

School of Physics, Northwest University, Xi'an 710069, China

* Correspondence: luo@nwu.edu.cn

Abstract: The classical two-step sol-gel hydrothermal method enables the growth of nanoarrays on various substrates via a seed layer. The morphology of the nanoarrays is often tuned by changing the composition ratio of the seed solution. It is taken for granted that the number density and size of seeds will increase with the proportion of precursors. However, in this work, we found novel two-stage dependencies between the concentration of the precursor (ZnAC) and the geometric parameters (number density and diameter) of ZnO seed particles. The completely opposite dependencies illustrate the existence of two different mechanisms. Especially when the proportion of precursors is low ($\phi_{ZnAC} : \phi_{PVA} < 0.22$), the seed number density and diameter decrease with the increasing precursor concentration. This counterintuitive phenomenon should be caused by the destabilization and dewetting process of the thin film layers during annealing. Based on this new mechanism, we demonstrate the tuning growth of the ZnO seed layer and the nanowire array by annealing time. The number density of the nanorod array can be changed by 10 times, and the diameter of the nanorods can be changed by more than 8 times. The new mechanism we proposed can not only help people deepen their understanding of the formation and evolution of the seed layer but also provide a new way for the controllable growth of nanomaterials.

Keywords: ZnO; nano-structure; dewetting



Citation: Li, Z.; Yan, N.; Tian, Y.; Luo, H. Tuning Growth of ZnO Nano-Arrays by the Dewetting of Gel Layer. *Crystals* **2023**, *13*, 30. <https://doi.org/10.3390/cryst13010030>

Academic Editor: Conrad Becker

Received: 22 November 2022

Revised: 7 December 2022

Accepted: 20 December 2022

Published: 24 December 2022



Copyright: © 2022 by the authors. Licensee MDPI, Basel, Switzerland. This article is an open access article distributed under the terms and conditions of the Creative Commons Attribution (CC BY) license (<https://creativecommons.org/licenses/by/4.0/>).

1. Introduction

Research on ZnO nanomaterials has been booming since the 1990s [1–6]. Due to its excellent characteristics, zinc oxide has always maintained a high degree of attention in the fields of energy, environment, biology, and detection [7–13]. In these decades of research, controllable growth and cost reduction are two aspects to which people have been committed. Among various growth methods, the sol-gel hydrothermal method has great potential for industrial application [14–16]. The sol-gel hydrothermal method is generally divided into two steps. The first step is to grow a seed layer on the target substrate using the sol-gel method, and the second step is to grow the nanomaterials on the seed layer by the hydrothermal method. This seed layer-based growth method is mostly used to prepare array structures. Due to the transition of the seed layer, nanomaterials can be grown on lattice-mismatched or even amorphous materials. At the same time, the hydrothermal method has relatively loose requirements on growth conditions and does not require a high-temperature environment, which is undoubtedly friendly to both substrates and equipment [17–22].

Since the geometric size of ZnO nanomaterials directly affects their performance in various aspects, such as solar power generation, photodegradation, self-cleaning, and antibacterial, people have always been enthusiastic about the controllable growth of nanomaterials [23–29]. When using the sol-gel hydrothermal method, the geometric size of the nanomaterials can be tuned in the first and second steps, respectively. In the second step of hydrothermal growth, what can be regulated is usually the size of the monomers that make up the array. In the process of preparing the seed layer in the first step, the size and density

of the seed can directly affect the structural parameters of the nanomaterial monomers and arrays [30–33]. Therefore, the geometric parameters of nanomaterials can be regulated from more dimensions through the seed layer. When preparing the seed sol, some polymers will be added to the solution as stabilizers. These macromolecules help form a more uniform film when the solution is coated on the substrate and are completely broken down during the annealing process. Since the temperature at which the precursor is transformed into a seed is different from the decomposition temperature of the polymer stabilizer, the dewetting kinetics during annealing can be exploited to tune the morphology of the seed layer. Müller et al. tuned the shape of gold particles at the nanoscale using the dewetting process of molten gold at high temperatures [34]. Martin et al. achieved highly localized control of pattern formation in two-dimensional nanoparticle assemblies by direct modification of solvent dewetting dynamics [35]. Their works imply that the dewetting process can effectively control the distribution and shape of nanoparticles in two-dimensional space. Huang et al. have reported that uniform single-crystalline nanowire arrays can be grown even on an amorphous seed layer made by low-temperature annealing [36]. This shows that the geometry of the seed layer is far more important than its own crystallinity. In other words, if the polymer stabilizer is not completely vaporized, the nanoparticles can still be used as crystallization nuclei to support the growth of nanomaterials. This implies that the gel layer containing the polymer will undergo a dewetting process from film rupture to complete crystallization during annealing. In this process, the size and distribution of the fragments of the film will change greatly, which means that the morphology of the seed layer will have a large adjustment range.

Therefore, we try to use the rupture and dewetting process of the gel film to achieve a wide range of controllable growth of nano-zinc oxide materials. Here, we used zinc acetate and PVA to prepare different ratios of seed layer solutions, spin-coated on silicon substrates and annealed to prepare ZnO seed layers. ZnO nanoarrays were then grown on the seed layer using a hydrothermal method. We systematically studied the film cracking and dewetting behavior of the gel layer with different precursor concentrations during the annealing process and confirmed the impact of these behaviors on the density of the seed layer/nanowire array by using atomic force microscopy, scanning electron microscopy, and dark field optical microscopy.

2. Materials and Methods

2.1. ZnO Seed Layer Preparation

The chemical materials used are from Alfa Aesar (Ward Hill, MA, USA) and are analytically pure. Silicon wafer substrates (1 cm × 1 cm) were carried out with ultrasonic cleaning in absolute ethanol for 20 min and with plasma cleaning for 5 min to make the surface hydrophilic before use. First, 2.5 g PVA (Mw 89,000–98,000, 99+% hydrolyzed) is dissolved in deionized water to prepare 50 mL PVA solution, with heating and stirring at 82 °C until the solution becomes clear. At the same time, different amounts of zinc acetate dihydrate are dissolved in a proper amount of deionized water to obtain 10 mL of solutions with zinc acetate concentrations of 0.01 g/mL, 0.02 g/mL, 0.04 g/mL, 0.08 g/mL, 0.16 g/mL, 0.26 g/mL, and 0.32 g/mL, respectively. Then, mix and stir 50 mL of PVA solution and 10 mL of zinc acetate solution for 2 h to obtain a sol seed solution. The seed solution is spin-coated on the cleaned silicon substrate at 5000 rpm (1000 rpm/s) for 2 min to obtain a gel layer. The heating plate was preheated to 500 °C to ensure a stable annealing temperature. Then heat the spin-coated sample in the air to form a seed layer.

2.2. ZnO Nanostructures Preparation

Hexamethylene tetramine, zinc nitrate hexahydrate, and ammonia water are used to prepare growth solution for hydrothermal reaction with the concentration of hexamethylene tetramine and zinc nitrate hexahydrate in the growth solution being both 0.1 mol/L. Add 12 mL of ammonia water to clarify the solution after 150 mL of the solution is prepared.

Place the prepared seed coating in the growth solution with growing at 90 °C for 6 h. Then the obtained array sample is washed with deionized water and dried in air.

2.3. Measurement Methods

Atomic force microscope (AFM, Dimension Icon, Bruker, MA, USA) and Scanning electron microscope (SEM, JSM-6700F, JEOL, Tokyo, Japan) were employed to characterize the morphology of the seed layer and nanoarrays, respectively. Dark-field microscopy (LV100, Nikon, Tokyo, Japan) was used to count the seed number density of the seed layer at different annealing times. The geometric parameters of the seeds and nanostructures were obtained using ImageJ from AFM, SEM, and dark-field microscopy images.

3. Results and Discussion

3.1. Morphology of Seed Layer

In order to present the proportion of ZnAC and PVA more intuitively, we express the solution of each seed layer by the ratio of the volume fractions, $\alpha = \phi_{ZnAC} : \phi_{PVA}$. After 40 min annealing at 500 °C, the seed layer samples were characterized by AFM, and the AFM images are shown in Figure 1. When α is relatively small (≤ 0.11), some obvious circular spots appear on the substrate, and the number of these spots increases with the alpha, but the diameter of each spot gradually decreases, as shown in Figure 1a–c. When the concentration of zinc acetate is further increased, those circular spots no longer appear, replaced by a granular film covering the entire substrate. Although the size of these particles gradually increases with the increase of alpha, overall, the particle film is very uniform, as shown in Figure 1d–g. Comparing the circular spots and particles, it can be seen that the size of the spots is larger than that of the particles, but the number of particles far exceeds that of the spots. Moreover, the change in their geometric parameters is relatively regular.

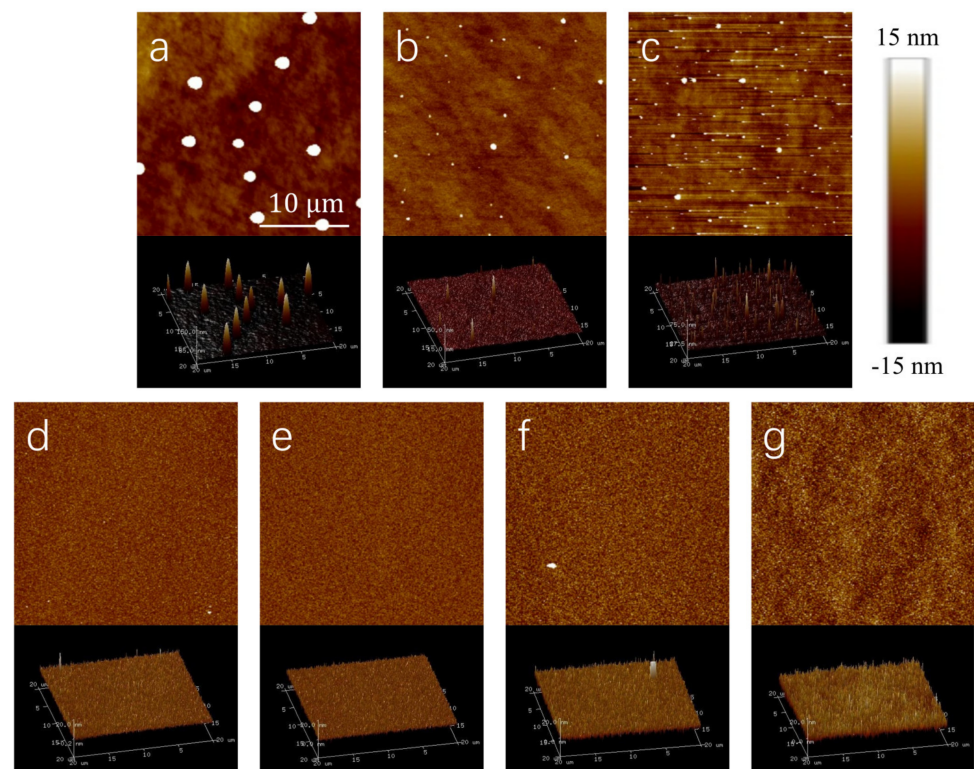


Figure 1. Typical AFM images of annealed seed layer with different ZnAC/PVA volume ratios. (a) 0.027:1, (b) 0.055:1, (c) 0.11:1, (d) 0.22:1, (e) 0.44:1, (f) 0.72:1 and (g) 0.87:1. The scanning range of each sample is $20 \times 20 \mu\text{m}^2$, and all images use the same scale bar.

As a seed layer, the protrusions on the surface will undoubtedly become the crystallization nuclei for the growth of nanomaterials, so these spots and particles (or be called the seeds) are the focus of our attention. To quantify changes in the morphology of the seed layer, we performed statistics on the number density and diameter of circular spots and particles. In Figure 2a, the change of seed number density with volume ratio can be clearly divided into two regions. Interestingly, in the first region, the number density of seeds increases with the ZnAC/PVA volume ratio, while in the second region, the relationship is negatively correlated. Figure 2b shows the change in seed diameter with α , which is also measured from the AFM image. AFM is very accurate for measuring height information perpendicular to the direction of the substrate, but it is too large for measuring dimensions parallel to the direction of the substrate. However, in our case, what we only need is the relative changes in seed diameter in different samples, so measurements based on AFM images are credible. It can be seen from Figure 2b the variation in seed diameter is also divided into two regions. In the first region, the seed diameter decreased rapidly with the increase in the volume ratio of ZnAC/PVA, while in the second region, the diameter of the seed increased slightly with the increase in the volume ratio. Here “slightly” is the reduction relative to the first region. Focus on the second region, the mean diameter of the seeds increased from 24 nm to 48 nm when the volume ratio of ZnAC/PVA increased from 0.22 to 0.87. It should be noted that both the absolute value of the number density and diameter of the seeds in the first region is much smaller than that in the second region. The opposite dependence and the large difference in number density imply that there are differences in the mechanism of seed formation in these two regions.

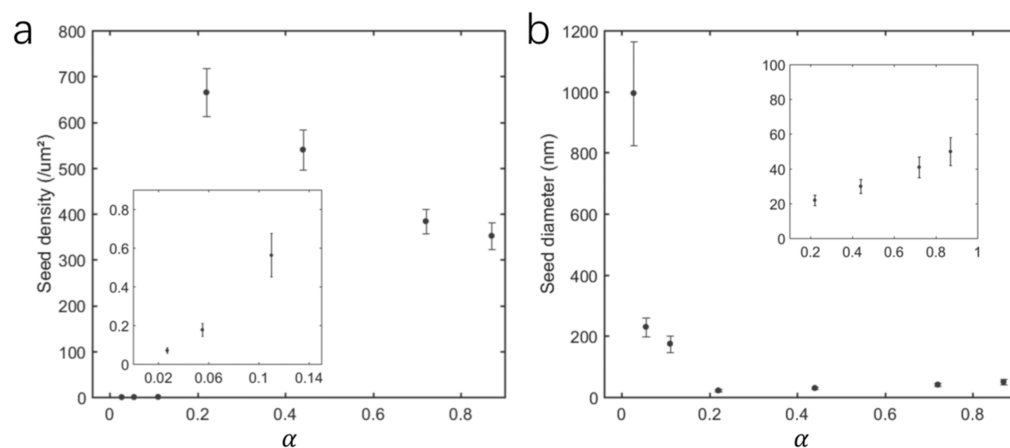


Figure 2. Variation of seed layer morphology parameters with ZnAC/PVA volume ratio α . (a,b) are statistics of the number density and diameter of seeds, respectively.

3.2. Morphology of Nanoarrays

Although the size of seeds has a very wide range of regulation, can the nanostructures grown based on seeds also have a corresponding dependence and regulation range? Each group of samples in Figure 1 was grown by the hydrothermal method under the same conditions for 6 h. SEM was employed to characterize the morphology of the nanoarrays, and typical images are shown in Figure 3. All samples exhibit nanorod/wire array morphology. It can be clearly seen that when α is low, the size of the grown nanorods is very uneven, and the directivity is not good, as shown in Figure 3a,b. When the α is increased to 0.11 and above, the uniformity and directivity of the array improve a lot.

To quantitatively investigate the relationship between the nanoarrays and the geometric parameters of the seed layer, we also analyzed the SEM images of the nanoarrays. Here the number density and tip diameter of nanorods were measured and counted. As shown in Figure 4, the number density of nanorods in the array shows a trend of increasing before decreasing with the increase of α , while the diameter of nanorods shows a trend of decreasing before increasing with the increase of α . The variation trend of the number

density and diameter of nanorods with alpha is consistent with that of the seed layer, as shown in Figure 2. Moreover, no matter whether it is the seed layer or the nano-array, the turning point, a critical ZnAC/PVA volume ratio α_c , separating the two regions, is between 0.11 and 0.22.

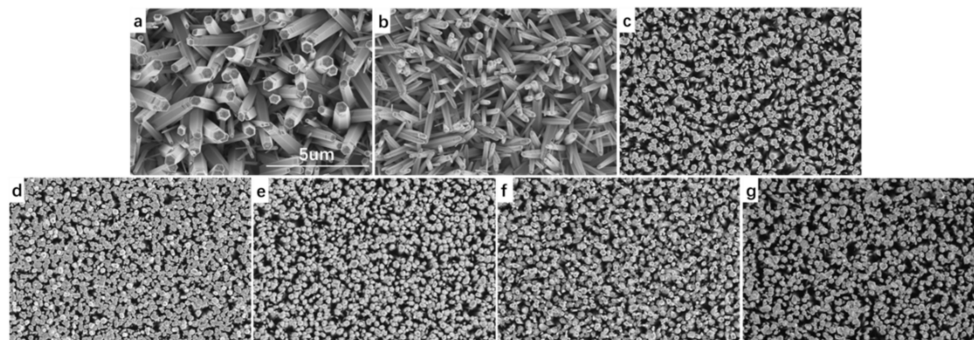


Figure 3. Typical SEM images of ZnO nanoarray based on the seed layer with different ZnAC/PVA volume ratios. (a) 0.027:1, (b) 0.055:1, (c) 0.11:1, (d) 0.22:1, (e) 0.44:1, (f) 0.72:1 and (g) 0.87:1. All images use the same scale bar.

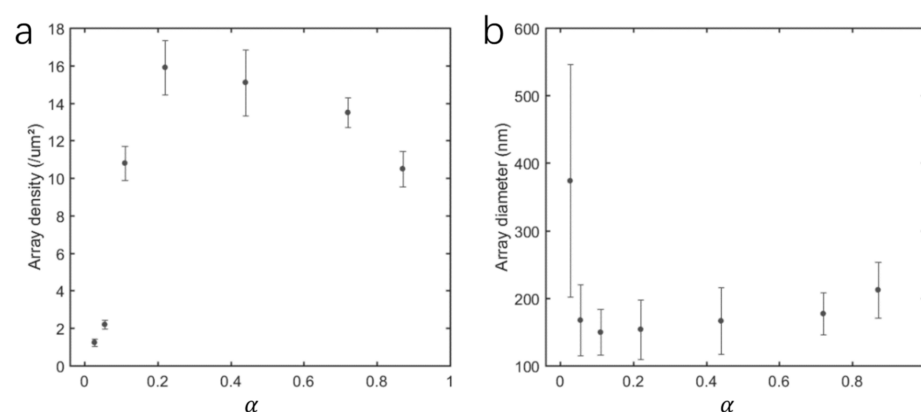


Figure 4. Variation of nanoarrays morphology parameters with ZnAC/PVA volume ratio α . (a) and (b) are statistics of the number density and diameter of nanorods, respectively.

Here are the following three points to note. (1) In the high α region, the average number density of nanorods is smaller than that of seeds because the adjacent structures will fuse at the early stage of nanomaterial growth. (2) In the low α region, the average number density and diameter of the nanorods are much larger and smaller than the seeds, respectively. This is most likely because the circular spots that appear on the seed layer in the low α region are not a single nucleation site, and due to their large size (diameter can reach 1 micron), it is likely that there are multiple nucleation sites on it. (3) In the low α region, the lower uniformity of ZnO nanoarray is likely to be due to the inhomogeneous distribution of ZnO nanoparticles converted from ZnAC actually used for nucleation. This inhomogeneous distribution is most likely caused by circular spots on the seed layer. The high-density ZnO particle aggregates will fuse into nanorods with larger diameters during the hydrothermal synthesis process.

3.3. Two Mechanisms for Seed Layer

Since the topography of the nanoarrays has a strong dependence on that of the seed layer, and the inhomogeneity of the nanoarrays in the low α region is likely to be caused by round spots on the seed layer, a question is raised: What are the round spots and how do they arise?

PVA accounted for more volume fraction in the ZnAV and PVA blended gel layer. Therefore, we can assume that the properties of the gel film are affected by PVA during

annealing, especially in the low α region. During the annealing process, the temperature of the substrate is gradually increased, so the PVA will first start to soften (glass transition temperature ~ 80 °C) before the temperature reaches the PVA decomposition temperature (200–250 °C). The softened film becomes unstable and then breaks up due to thermal disturbances. The broken film shrinks under the action of surface tension, which is known as dewetting. This will leave circular spots on the substrate. During the dewetting process, the boundaries of the circular spots shrink gradually, leaving ZnAC molecules or converted ZnO in the shrinking path. However, as the shrinkage rate increases with temperature, the concentration of Zn atoms in the spots is also gradually concentrated, which leads to the uneven density of nucleation sites left on the surface of the substrate, and in turn, affects the uniformity of the subsequently grown nanoarrays. Moreover, when the α is higher, the properties of the gel film gradually tend to zinc acetate. The softening degree of the membrane will gradually decrease, and it is not easy to become unstable and broken under the action of thermal disturbance. Therefore, a ZnO seed layer with small particles and uniform distribution can be formed.

3.4. Dewetting Tuned Nanoarray Growth

In order to verify our conjecture and try to use dewetting to regulate the morphology of the seed layer and nanoarray, we designed the following experiments. Two sets of samples below and one set above the critical ZnAC/PVA volume ratio α_c were selected, which were $\alpha = 0.027, 0.11$ and 0.44 . Each group of samples was annealed on a hot plate at 500 °C for 10 min, 40 min, and 80 min, respectively. The surface morphology of the annealed samples was observed using a dark-field microscope. Then these samples will undergo hydrothermal reaction in the same environment to grow nano-arrays, and the nano-arrays will be characterized by SEM.

Here we mainly focus on the rupture and dewetting process of the gel film. Due to the large size of the circular spot after the gel film rupture and poor conductivity, AFM and SEM are not applicable. The dark-field microscope is very sensitive to surface fluctuations and is very suitable for observing the breaking process of the gel film. As shown in Figure 5, the bright spots in the images indicate that there is a difference between the height of this position and the base. During the annealing process, a large number of particles appeared in the two samples with low α , while the sample $\alpha = 0.44$ did not change significantly throughout the annealing process. For the two sets of samples with low α , there are changes both in the diameter and number of particles. Since the dark field microscope cannot accurately characterize the size of the particles, here we mainly analyze the number density of the particles.

As shown in Figure 6, as the annealing time increases, the number density of the surface particles of the two groups of low α samples first increases and then decreases. This two-stage trend corresponds to the gradual rupture of the film, and more and more “islands” are split, and as the annealing time increases, the residual PVA is gradually decomposed, and the size of the islands is constantly shrinking. This two-stage trend means that the film splits more and more particles during the gradual rupture process at the beginning. Then as the annealing time increases, the PVA is gradually decomposed, and the size of the particles continues to shrink. The particles will gradually disappear from small to large until the PVA is completely decomposed and only ZnO particles remain. Another interesting phenomenon is that the number density of particles on the $\alpha = 0.11$ sample is larger than that of $\alpha = 0.027$, and at 80 min, when the number density of $\alpha = 0.027$ has returned to a small value, the number density of $\alpha = 0.11$ is still increasing. This phenomenon is consistent with the results of AFM. The reasons for this phenomenon are multifaceted and complex. It may be because the increase in the volume fraction of zinc acetate changes the viscosity, surface tension of the solution, the stiffness of the film after softening, and so on.

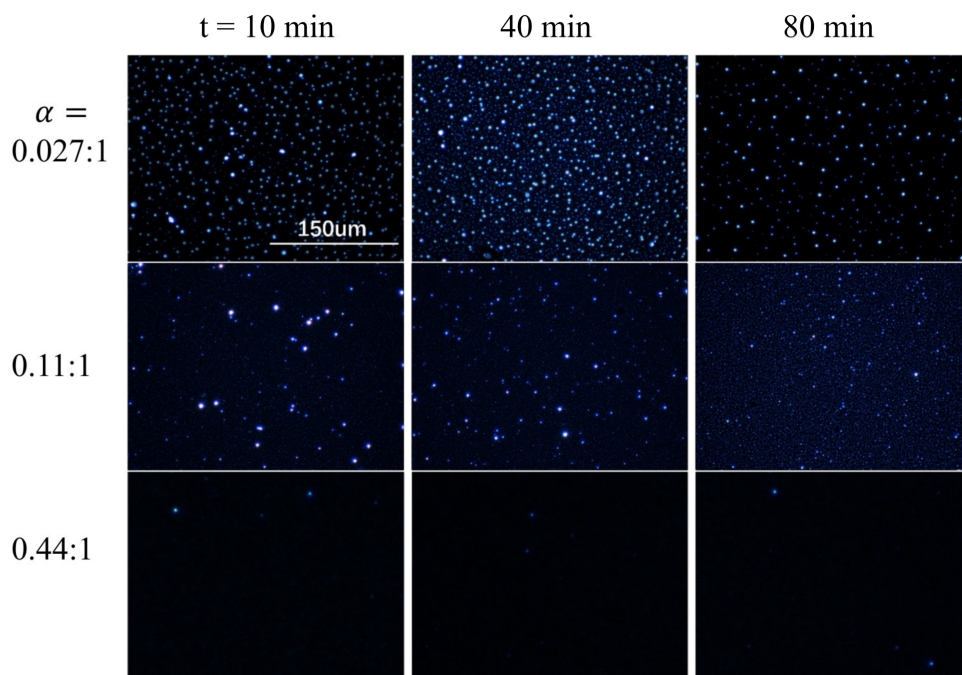


Figure 5. Dark field microscope images of gel layers with different alpha values after different annealing times.

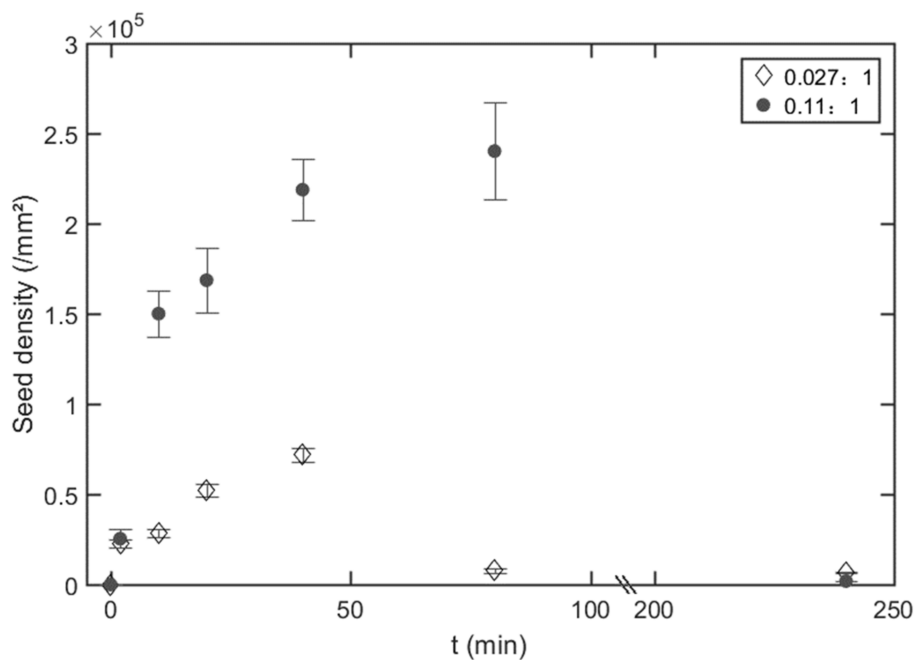


Figure 6. Variation of number density of particles with annealing time.

Since the process of dewetting after gel film rupture can be controlled by the annealing time, the nanoarrays grown based on the seed layer must also be controlled. The ZnO nanoarrays shown in Figure 7 were obtained by hydrothermal growth of the seed layer in Figure 6 under the same conditions. The large difference in morphology of samples α = 0.027 and the stability of sample α = 0.44 are in line with expectations obtained from their seed layer. However, for sample α = 0.11, the difference between the seed layer annealed for 40 min and 80 min is not obvious on the ZnO array. This means that when the number density of seeds is greater than a certain value, the nanoarray is no longer sensitive to the number density of seeds. The same conclusion can be obtained more intuitively from statistical data, as shown in Figure 8. For a high α sample (α = 0.44), array uniformity is

better, but tunability is lost. The sample $\alpha = 0.11$ is more balanced, with good uniformity and some tunability. If the effect of A and annealing time is considered comprehensively, the number density of the nanorod array can be changed by 10 times ($2\sim 20/\mu\text{m}^2$), and the diameter of the nanorods can be changed by more than 8 times ($50\sim 400\text{ nm}$).

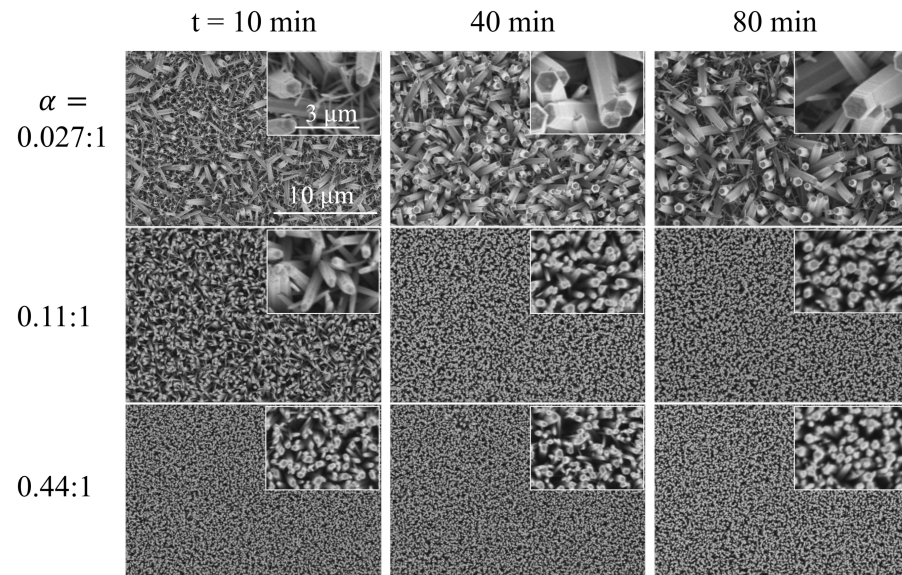


Figure 7. SEM images of nanoarrays obtained by different zinc acetate/PVA volume ratios and annealing times.

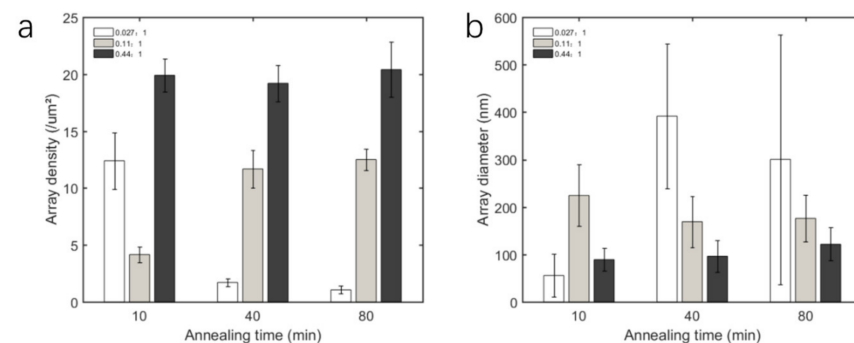


Figure 8. Variation of nanoarrays morphology parameters with ZnAC/PVA volume ratio α and annealing time. (a,b) are statistics of the number density and diameter of nanorods, respectively.

It is true that the dewetting process of seeds can regulate the morphology of nanoarrays, but in reverse thinking, when we want the product to have high stability, we should try to avoid the occurrence of the de-wetting process, that is, choose a high alpha value. However, if high alpha cannot be selected; for example, the precursor is very expensive, and we have to pay more patience to let the dewetting process be completed.

4. Conclusions

In summary, based on the classical sol-gel hydrothermal method, we systematically investigated the effect of the volume ratio α between the precursor ZnAC and the stabilizer PVA in the seed layer solution on the morphology of seeds and nanoarrays. We found that there are two mechanisms in the annealing process of the seed layer. When alpha is less than or equal to 0.22, the fragmentation and dewetting process of the gel film is crucial, and the morphology of the seed layer and nanoarray is very sensitive to alpha; when alpha is greater than or equal to 0.44, the gel film will not be broken, and the morphology of the seed layer and nano-array will only change slightly with alpha. In addition, by adjusting the annealing time, we controlled the dewetting process of the seed layer and then successfully

regulated the morphology of the nanoarrays. The number density of the nanorod array can be changed from $2/\mu\text{m}^2$ to $20/\mu\text{m}^2$, and the diameter of the nanorods can be changed from 50 nm to 400 nm. Our work demonstrates that the film rupture and dewetting process is an important mechanism in the formation of the seed layer by the sol-gel method. This not only helps people to complete the understanding of the mechanism of the sol-gel hydrothermal method but also provides an important reference for the controllable growth of nanomaterials.

Author Contributions: Conceptualization, Z.L., N.Y. and H.L.; methodology, Z.L., N.Y. and H.L.; software, Z.L. and H.L.; investigation, N.Y., Y.T. and H.L.; resources, Z.L.; data curation, Z.L.; writing—review and editing, N.Y., Y.T. and H.L.; supervision, N.Y., Y.T. and H.L.; project administration, N.Y., Y.T. and H.L.; funding acquisition, H.L.; All authors have read and agreed to the published version of the manuscript.

Funding: This research received funding from National Natural Science Foundation of China (61902316).

Institutional Review Board Statement: Not applicable.

Informed Consent Statement: Not applicable.

Data Availability Statement: Not applicable.

Acknowledgments: The authors gratefully acknowledge the help from P. Li.

Conflicts of Interest: The authors declare no conflict of interest.

References

1. Zhang, H.; Ma, X.; Xu, J.; Niu, J.; Yang, D. Arrays of ZnO nanowires fabricated by a simple chemical solution route. *Nanotechnology* **2003**, *14*, 423. [[CrossRef](#)]
2. Greyson, E.C.; Babayan, Y.; Odom, T.W. Directed growth of ordered arrays of small-diameter ZnO nanowires. *Adv. Mater.* **2004**, *16*, 1348–1352. [[CrossRef](#)]
3. Fan, H.J.; Lee, W.; Scholz, R.; Dadgar, A.; Krost, A.; Nielsch, K.; Zacharias, M. Arrays of vertically aligned and hexagonally arranged ZnO nanowires: A new template-directed approach. *Nanotechnology* **2005**, *16*, 913. [[CrossRef](#)]
4. Weintraub, B.; Zhou, Z.; Li, Y.; Deng, Y. Solution synthesis of one-dimensional ZnO nanomaterials and their applications. *Nanoscale* **2010**, *2*, 1573–1587. [[CrossRef](#)]
5. Zhu, P.; Weng, Z.; Li, X.; Liu, X.; Wu, S.; Yeung, K.; Wang, X.; Cui, Z.; Yang, X.; Chu, P.K. Biomedical applications of functionalized ZnO nanomaterials: From biosensors to bioimaging. *Adv. Mater. Interfaces* **2016**, *3*, 1500494. [[CrossRef](#)]
6. Le Pivert, M.; Poupard, R.; Capochichi-Gnambodoe, M.; Martin, N.; Leprince-Wang, Y. Direct growth of ZnO nanowires on civil engineering materials: Smart materials for supported photodegradation. *Microsyst. Nanoeng.* **2019**, *5*, 57. [[CrossRef](#)]
7. Le Pivert, M.; Piebourg, A.; Bastide, S.; Duc, M.; Leprince-Wang, Y. Direct One-Step Seedless Hydrothermal Growth of ZnO Nanostructures on Zinc: Primary Study for Photocatalytic Roof Development for Rainwater Purification. *Catalysts* **2022**, *12*, 1231. [[CrossRef](#)]
8. Wang, J.; Chen, R.; Xiang, L.; Komarneni, S. Synthesis, properties and applications of ZnO nanomaterials with oxygen vacancies: A review. *Ceram. Int.* **2018**, *44*, 7357–7377. [[CrossRef](#)]
9. Rong, P.; Ren, S.; Yu, Q. Fabrications and applications of ZnO nanomaterials in flexible functional devices—a review. *Crit. Rev. Anal. Chem.* **2019**, *49*, 336–349. [[CrossRef](#)]
10. Chaudhary, S.; Umar, A.; Bhasin, K.; Baskoutas, S. Chemical sensing applications of ZnO nanomaterials. *Materials* **2018**, *11*, 287. [[CrossRef](#)]
11. Djurišić, A.B.; Chen, X.; Leung, Y.H.; Ng, A.M.C. ZnO nanostructures: Growth, properties and applications. *J. Mater. Chem.* **2012**, *22*, 6526–6535. [[CrossRef](#)]
12. Theerthagiri, J.; Salla, S.; Senthil, R.; Nithyadharseni, P.; Madankumar, A.; Arunachalam, P.; Maiyalagan, T.; Kim, H.-S. A review on ZnO nanostructured materials: Energy, environmental and biological applications. *Nanotechnology* **2019**, *30*, 392001. [[CrossRef](#)]
13. Kumar, R.; Umar, A.; Kumar, G.; Nalwa, H.S. Antimicrobial properties of ZnO nanomaterials: A review. *Ceram. Int.* **2017**, *43*, 3940–3961. [[CrossRef](#)]
14. Khan, M.F.; Ansari, A.H.; Hameedullah, M.; Ahmad, E.; Husain, F.M.; Zia, Q.; Baig, U.; Zaheer, M.R.; Alam, M.M.; Khan, A.M. Sol-gel synthesis of thorn-like ZnO nanoparticles endorsing mechanical stirring effect and their antimicrobial activities: Potential role as nano-antibiotics. *Sci. Rep.* **2016**, *6*, 1–12. [[CrossRef](#)]
15. Al Abdullah, K.; Awad, S.; Zaraket, J.; Salame, C. Synthesis of ZnO nanopowders by using sol-gel and studying their structural and electrical properties at different temperature. *Energy Procedia* **2017**, *119*, 565–570. [[CrossRef](#)]

16. Torres, F.D.C.G.; López, J.L.C.; Rodríguez, A.S.L.; Gallardo, P.S.; Morales, E.R.; Hernández, G.P.; Guillen, J.C.D.; Flores, L.L.D. Sol-gel/hydrothermal synthesis of well-aligned ZnO nanorods. *Boletín Soc. Española Cerámica Y Vidr.* 2022; *in press*.
17. Zhang, J.; Que, W. Preparation and characterization of sol-gel Al-doped ZnO thin films and ZnO nanowire arrays grown on Al-doped ZnO seed layer by hydrothermal method. *Sol. Energy Mater. Sol. Cells* **2010**, *94*, 2181–2186. [[CrossRef](#)]
18. Tian, J.-H.; Hu, J.; Li, S.-S.; Zhang, F.; Liu, J.; Shi, J.; Li, X.; Tian, Z.-Q.; Chen, Y. Improved seedless hydrothermal synthesis of dense and ultralong ZnO nanowires. *Nanotechnology* **2011**, *22*, 245601. [[CrossRef](#)]
19. Bai, S.-N.; Wu, S.-C. Synthesis of ZnO nanowires by the hydrothermal method, using sol-gel prepared ZnO seed films. *J. Mater. Sci. Mater. Electron.* **2011**, *22*, 339–344. [[CrossRef](#)]
20. Chevalier-César, C.; Capochichi-Gnambodoe, M.; Leprince-Wang, Y. Growth mechanism studies of ZnO nanowire arrays via hydrothermal method. *Appl. Phys. A* **2014**, *115*, 953–960. [[CrossRef](#)]
21. Zhang, Z.; Lv, Y.; Yan, J.; Hui, D.; Yun, J.; Zhai, C.; Zhao, W. Uniform ZnO nanowire arrays: Hydrothermal synthesis, formation mechanism and field emission performance. *J. Alloy. Compd.* **2015**, *650*, 374–380. [[CrossRef](#)]
22. Alshehri, N.A.; Lewis, A.R.; Pleydell-Pearce, C.; Maffei, T.G. Investigation of the growth parameters of hydrothermal ZnO nanowires for scale up applications. *J. Saudi Chem. Soc.* **2018**, *22*, 538–545. [[CrossRef](#)]
23. Tokumoto, M.S.; Pulcinelli, S.H.; Santilli, C.V.; Briois, V. Catalysis and temperature dependence on the formation of ZnO nanoparticles and of zinc acetate derivatives prepared by the sol-gel route. *J. Phys. Chem. B* **2003**, *107*, 568–574. [[CrossRef](#)]
24. Tak, Y.; Yong, K. Controlled growth of well-aligned ZnO nanorod array using a novel solution method. *J. Phys. Chem. B* **2005**, *109*, 19263–19269. [[CrossRef](#)] [[PubMed](#)]
25. Hossain, M.; Zhang, Z.; Takahashi, T. Novel micro-ring structured ZnO photoelectrode for dye-sensitized solar cell. *Nano-Micro Lett.* **2010**, *2*, 53–55. [[CrossRef](#)]
26. Evans, J.E.; Jungjohann, K.L.; Browning, N.D.; Arslan, I. Controlled growth of nanoparticles from solution with in situ liquid transmission electron microscopy. *Nano Lett.* **2011**, *11*, 2809–2813. [[CrossRef](#)] [[PubMed](#)]
27. Blandin, P.; Maximova, K.A.; Gongalsky, M.B.; Sanchez-Royo, J.F.; Chirvony, V.S.; Sentis, M.; Timoshenko, V.Y.; Kabashin, A.V. Femtosecond laser fragmentation from water-dispersed microcolloids: Toward fast controllable growth of ultrapure Si-based nanomaterials for biological applications. *J. Mater. Chem. B* **2013**, *1*, 2489–2495. [[CrossRef](#)] [[PubMed](#)]
28. Harish, V.; Ansari, M.M.; Tewari, D.; Gaur, M.; Yadav, A.B.; García-Betancourt, M.-L.; Abdel-Haleem, F.M.; Bechelany, M.; Barhoum, A. Nanoparticle and Nanostructure Synthesis and Controlled Growth Methods. *Nanomaterials* **2022**, *12*, 3226. [[CrossRef](#)]
29. He, Z.; Zhang, Z.; Bi, S. Nanoparticles for organic electronics applications. *Mater. Res. Express* **2020**, *7*, 012004. [[CrossRef](#)]
30. Baruah, S.; Dutta, J. Effect of seeded substrates on hydrothermally grown ZnO nanorods. *J. Sol-Gel Sci. Technol.* **2009**, *50*, 456–464. [[CrossRef](#)]
31. Chen, C.-L.; Rosi, N.L. Preparation of unique 1-D nanoparticle superstructures and tailoring their structural features. *J. Am. Chem. Soc.* **2010**, *132*, 6902–6903. [[CrossRef](#)]
32. Prieto, P.; Nistor, V.; Nouneh, K.; Oyama, M.; Abd-Lefdil, M.; Díaz, R. XPS study of silver, nickel and bimetallic silver-nickel nanoparticles prepared by seed-mediated growth. *Appl. Surf. Sci.* **2012**, *258*, 8807–8813. [[CrossRef](#)]
33. Lee, W.C.; Fang, Y.; Kler, R.; Canciani, G.E.; Draper, T.C.; Al-Abdullah, Z.T.; Alfadul, S.M.; Perry, C.C.; He, H.; Chen, Q. Marangoni ring-templated vertically aligned ZnO nanotube arrays with enhanced photocatalytic hydrogen production. *Mater. Chem. Phys.* **2015**, *149*, 12–16. [[CrossRef](#)]
34. Müller, C.M.; Mornaghini, F.C.F.; Spolenak, R. Ordered arrays of faceted gold nanoparticles obtained by dewetting and nanosphere lithography. *Nanotechnology* **2008**, *19*, 485306. [[CrossRef](#)] [[PubMed](#)]
35. Martin, C.P.; Blunt, M.O.; Pauliac-Vaujour, E.; Stannard, A.; Moriarty, P.; Vancea, I.; Thiele, U. Controlling pattern formation in nanoparticle assemblies via directed solvent dewetting. *Phys. Rev. Lett.* **2007**, *99*, 116103. [[CrossRef](#)]
36. Huang, J.-S.; Lin, C.-F. Influences of ZnO sol-gel thin film characteristics on ZnO nanowire arrays prepared at low temperature using all solution-based processing. *J. Appl. Phys.* **2008**, *103*, 014304. [[CrossRef](#)]

Disclaimer/Publisher’s Note: The statements, opinions and data contained in all publications are solely those of the individual author(s) and contributor(s) and not of MDPI and/or the editor(s). MDPI and/or the editor(s) disclaim responsibility for any injury to people or property resulting from any ideas, methods, instructions or products referred to in the content.